Supplementary Information

Transition Metal-based Coordination Polymers of Bipyridyl-ethylene for Sunlight-Driven Photocatalytic CO_2 Reduction into CO

A. Abidi, [a, b, c*] T.A. Quach,[d] M. Essalhi,[a, b, e] D. Chartrand,[f] T. O. Do,[d] S. Barnabé,[a, b, c*] M. Cibian[a, b*]

[a]*Département de biochimie, chimie, physique et science forensique, Université du Québec à Trois-Rivières, Trois-Rivières, Québec, G9A 5H7, Canada*
[b]*Institut de recherche sur l'hydrogène (IRH), Université du Québec à Trois-Rivières, Trois-Rivières, Québec, G9A 5H7, Canada*
[c]*Institut d'innovations en écomatériaux, écoproduits et écoénergies à base de biomasse (I2E3), Université du Québec à Trois-Rivières, Trois-Rivières, Québec, G9A 5H7, Canada*
[d]*Département de génie chimique, Université de Laval, Québec, Québec G1V 0A6, Canada*
[e]*Interdisciplinary Research Center for Hydrogen Technologies and Carbon Management, King Fahd University of Petroleum & Minerals, Dhahran 31261, Saudi Arabia*
[f]*Département de chimie, Université de Montréal, Montréal, Québec, H3C 3J7, Canada*

*To whom correspondence should be addressed. E-mail: adela.abidi@uqtr.ca / simon.barnabe@uqtr.ca mihaela.cibian@uqtr.ca

Table of content

1. Materials 4
2. Characterization 4
3. Hirshfeld Surface Analysis (HS) 16
4. Optical properties 17
5. Photoelectrochemical characterization 19
6. Photocatalytic CO_2 reduction 21
7. References 26

Table S1. Crystallographic Data and structure refinement details for **CoBpe**, **NiBpe** and **CuBpe** 4
Table S2. Bond lengths (Å) observed for **CoBpe** 5
Table S3. Bond angles (°) observed for **CoBpe** 6
Table S4. Hydrogen bond geometry (Å, º) for **CoBpe** 7
Table S5. Bond lengths (Å) observed for **NiBpe** 7
Table S6. Bond angles (º) observed for **NiBpe** 8
Table S7. Hydrogen bond geometry (Å, º) for **NiBpe** 9
Table S8. Bond lengths (Å) observed for **CuBpe** 10
Table S9. Bond angles (º) observed for **CuBpe** 10
Table S10. Control experiments performed to characterize the activity of **CoBpe** as a catalyst for photocatalytic reduction of CO_2 23
Table S11. CO production rates for selected relevant reported material-based photocatalytic systems 24

Fig. S1 The solid-state structure of **CoBpe** (ORTEP view, ellipsoid at 50% probability level) with labeled atoms. 12
Fig. S2 The solid-state structure of **NiBpe** (ORTEP view, ellipsoid at 50% probability level) with labeled atoms. 12
Fig. S3 The solid-state structure of **CuBpe** (ORTEP view, ellipsoid at 50% probability level) with labeled atoms. 13
Fig. S4 The solid-state structures of isostructural **CoBpe** and **NiBpe**: a) asymmetric unit (middle), coordination environment of Co(II) cation in **CoBpe** (left & right); b) asymmetric unit (middle), coordination environment of Ni(II) cation in **NiBpe** (left & right); c) view along a-axis showing interpenetrated ladders structure : each square grid is interpenetrated with two squares belonging to two other ladders (green & blue) resulting in an overall 3D network d) side view of the 3D ladder structure highlighting the interpenetration of the ladders. 13

Fig. S5 The solid-state structure of **CuBpe**: a) asymmetric unit (right) and coordination environment of Cu(II) cation (left); b) view along a-axis showing periodically alternating 1D channels (green & blue); c) view along c-axis showing the arrangement of 1D channels into 2D layers; d) view along b-axis showing the alternation of 1D channels. 14
Fig. S6 Experimental powder X-ray diffraction (PXRD) patterns of **CoBpe** (pink), **NiBpe** (green) and **CuBpe** (blue) – comparison with simulated patterns calculated from the corresponding single-crystal structure (in black). 15
Fig. S7 2D fingerprint plots with relative contributions (in percentage) of various intermolecular contacts to HS area for **CoBpe**. 16
Fig. S8 2D fingerprint plots with relative contributions (in percentage) of various intermolecular contacts to HS area for **NiBpe**. 16
Fig. S9 2D fingerprint plots with relative contributions (in percentage) of various intermolecular contacts to HS area for **CuBpe**. 17
Fig. S10 Tauc's plots for **CoBpe** (pink), **NiBpe** (green) and **CuBpe** (blue). 18
Fig. S11 Linear sweep voltammetry (LSV) curves for **Bpe** (black), **NiBpe** (green), **CoBpe** (pink), **CuBpe** (blue). 19
Fig. S12 Nyquist plots for **Bpe** (black), **NiBpe** (green), **CoBpe** (pink), **CuBpe** (blue). 19
Fig. S13 Mott-Schottky analysis for **CoBpe** (pink), **NiBpe** (green), **CuBpe** (blue). 20
Fig. S14 Electron-transfer diagram for **NiBpe** (a) and **CuBpe** (b), respectively.[3] 21
Fig. S15 Photocatalytic experiment: description, conditions, and setup. 21
Fig. S16 CO/H_2 production rates for **CoBpe** (top left), **NiBpe** (top right) and **CuBpe** (bottom) as a function of mass of catalyst; 4 hours of simulated sunlight irradiation; $[Ru(bpy)_3]Cl_2 \cdot 6H_2O$ (7.4 mg); $MeCN/H_2O$/TEOA (3/1/1, 10 mL); Experiments were performed at least in duplicate, and the error (1-15%) represents the standard deviation for repeated measurements. 22
Fig. S17 Photocatalytic CO and H_2 production for **CoBpe**, **NiBpe**, and **CuBpe** (10 mg); 4 hours of simulated sunlight irradiation; $[Ru(bpy)_3]Cl_2 \cdot 6H_2O$ (7.4 mg); $MeCN/H_2O$/TEOA (3/1/1, 10 mL); Experiments were performed at least in duplicate, and the error (1-15%) represents the standard deviation for repeated measurements. 22
Fig. S18 Proposed photocatalytic mechanism for CO_2 to CO conversion – exemplified for **CoBpe**. 25

1. Materials

Chemicals. Trans-1,2-Bis(4-pyridyl)ethylene (Bpe), cobalt nitrate hexahydrate ($Co(NO_3)_2 \cdot 6H_2O$), nickel nitrate hexahydrate ($Ni(NO_3)_2 \cdot 6H_2O$), copper perchlorate hexahydrate ($Cu(ClO_4)_2 \cdot 6H_2O$), tris(2,2′-bipyridyl)dichlororuthenium(II) hexahydrate $[Ru(bpy)_3]Cl_2 \cdot 6H_2O$, acetonitrile (MeCN), methanol (CH_3OH), and triethanolamine (TEOA) were purchased from Sigma-Aldrich, CO_2 gas of 99.99% in purity was provided by Praxair.

2. Characterization

Single-crystal X-ray diffraction (SCXRD)

Crystal data and structure refinement details for **CoBpe**, **NiBpe** and **CuBpe** are given in Table S1. The values for bond lengths, angles, and H-bonding geometry are presented in Tables S2-S9.

Table S1. Crystallographic Data and structure refinement details for **CoBpe**, **NiBpe** and **CuBpe**

Identification code	**CoBpe**	**NiBpe**	**CuBpe**
Empirical formula	$C_{37}H_{34}Co_2N_{10}O_{13}$	$C_{37}H_{34}N_{10}Ni_2O_{13}$	$C_{10}H_{11}CuNO_4$
Formula weight	944.608	944.16	272.74
Temperature/K	100.00	150	150
Crystal system	Monoclinic	Monoclinic	Triclinic
Space group	$P2_1/c$	$P2_1/c$	P-1
a/Å	16.7702(2)	16.4935(4)	7.4818(4)
b/Å	14.7182(2)	14.9543(4)	8.4377(5)
c/Å	16.6433(2)	16.5573(4)	9.7327(6)
α/°	90	90	98.578(3)
β/°	93.4334(12)	93.8480(10)	111.346(2)
γ/°	90	90	104.415(2)
Volume/Å^3	4100.66(9)	4074.63(18)	534.31(5)
Z	4	4	2
ρ_{calc}g/cm^3	1.530	1.539	1.695
μ/mm^{-1}	0.886	5.480	11.050
F(000)	1940.4	1944.0	278.0
Crystal size/mm^3	0.2 × 0.15 × 0.1	0.185 × 0.15 × 0.09	0.099 × 0.056 × 0.03
Radiation	Mo Kα (λ = 0.71073)	Ga Kα (λ = 1.34139)	Ga Kα (λ = 1.34139)
2Θ range for data collection/°	5.54 to 59.06	4.672 to 132.198	8.804 to 131.632
Index ranges	-21 ≤ h ≤ 20, -19 ≤ k ≤ 19, -21 ≤ l ≤ 22	-21 ≤ h ≤ 22, -20 ≤ k ≤ 18, -22 ≤ l ≤ 20	-10 ≤ h ≤ 9, -11 ≤ k ≤ 11, 0 ≤ l ≤ 13
Reflections collected	31081	60624	2596
Independent reflections	9664 [R_{int} = 0.0286, R_{sigma} = 0.0357]	10276 [R_{int} = 0.0479, R_{sigma} = 0.0339]	2596 [R_{int} = 0.0479, R_{sigma} = 0.0323]
Data/restraints/parameters	9664/0/699	10276/0/562	2596/176/230
Goodness-of-fit on F^2	1.062	1.024	1.056

Final R indexes [I>=2σ (I)]	R_1 = 0.0333, wR_2 = 0.0728	R_1 = 0.0344, wR_2 = 0.0824	R_1 = 0.0319, wR_2 = 0.0824
Final R indexes [all data]	R_1 = 0.0503, wR_2 = 0.0826	R_1 = 0.0456, wR_2 = 0.0869	R_1 = 0.0350, wR_2 = 0.0838
Largest diff. peak/hole / e $Å^{-3}$	0.67/-0.54	0.36/-0.44	0.31/-0.46

Table S2. Bond lengths (Ǻ) observed for **CoBpe**

Atom	Atom	Length/Å	Atom	Atom	Length/Å
Co1	O1	2.0504(14)	C2	C4	1.382(3)
Co1	O2	2.2061(13)	C3	C5	1.392(3)
Co1	O3	2.1025(13)	C4	C5	1.396(3)
Co1	N1	2.1154(15)	C5	C17	1.466(2)
Co1	N4	2.1398(15)	C6	C16	1.377(3)
Co1	N5	2.1353(15)	C7	C8	1.472(2)
Co2	O5	2.1472(15)	C7	C17	1.334(3)
Co2	O6	2.2314(14)	C8	C9	1.395(3)
Co2	O8	2.0380(15)	C8	C10	1.394(3)
Co2	N2	2.1234(15)	C9	C12	1.387(3)
Co2	N6	2.1531(15)	C10	C11	1.379(3)
Co2	N7	2.1026(15)	C13	C14	1.382(3)
O1	C36	1.434(2)	C14	C15	1.392(3)
O2	N3	1.273(2)	C15	C16	1.394(3)
O3	N3	1.274(2)	C15	C241	1.461(3)
O4	N9	1.236(2)	C18	C21	1.378(3)
O5	N8	1.282(2)	C19	C20	1.380(3)
O6	N8	1.269(2)	C20	C22	1.400(2)
O7	N8	1.222(2)	C21	C22	1.395(2)
O8	N9	1.289(2)	C22	C23	1.465(2)
O9	N9	1.230(2)	C23	C24	1.336(3)
O10	N3	1.222(2)	C25	C28	1.380(3)
N1	C1	1.345(2)	C26	C27	1.381(3)
N1	C2	1.345(2)	C27	C29	1.395(3)
N2	C11	1.346(2)	C28	C29	1.395(3)
N2	C12	1.345(2)	C29	C30	1.467(3)
N4	C25	1.348(2)	C30	C31	1.331(3)
N4	C26	1.347(2)	C31	C32	1.468(3)
N5	C18	1.348(2)	C32	C33	1.395(3)
N5	C19	1.341(2)	C32	C34	1.393(3)
N6	C6	1.342(3)	C33	C502	1.376(3)
N6	C13	1.342(2)	C34	C462	1.374(3)
N7	C46	1.345(2)	O11	N10	1.283(2)
N7	C50	1.346(2)	O12	N10	1.233(2)
C1	C3	1.378(3)	O13	N10	1.245(2)

[1]1-X,1-Y,1-Z; 22-X,-Y,2-Z

Table S3. Bond angles (°) observed for **CoBpe**

Atom	Atom	Atom	Angle/°	Atom	Atom	Atom	Angle/°
O2	Co1	O1	98.54(5)	O6	N8	O5	116.15(16)
O3	Co1	O1	158.55(5)	O7	N8	O5	120.87(18)
O3	Co1	O2	60.18(5)	O7	N8	O6	122.97(17)
N1	Co1	O1	103.69(6)	O8	N9	O4	117.57(17)
N1	Co1	O2	157.73(6)	O9	N9	O4	123.90(18)
N1	Co1	O3	97.55(5)	O9	N9	O8	118.53(18)
N4	Co1	O1	90.68(6)	C3	C1	N1	123.30(18)
N4	Co1	O2	91.08(5)	C4	C2	N1	122.96(18)
N4	Co1	O3	92.38(6)	C5	C3	C1	119.74(18)
N4	Co1	N1	89.84(6)	C5	C4	C2	119.80(18)
N5	Co1	O1	88.54(6)	C4	C5	C3	117.01(17)
N5	Co1	O2	87.38(5)	C17	C5	C3	124.05(17)
N5	Co1	O3	87.74(6)	C17	C5	C4	118.92(17)
N5	Co1	N1	91.97(6)	C16	C6	N6	123.65(19)
N5	Co1	N4	178.15(6)	C17	C7	C8	122.82(18)
O6	Co2	O5	59.24(5)	C9	C8	C7	120.84(17)
O8	Co2	O5	171.09(5)	C10	C8	C7	121.88(17)
O8	Co2	O6	112.12(6)	C10	C8	C9	117.28(17)
N2	Co2	O5	100.49(6)	C12	C9	C8	119.55(18)
N2	Co2	O6	158.40(6)	C11	C10	C8	119.64(18)
N2	Co2	O8	87.73(6)	C10	C11	N2	123.33(18)
N6	Co2	O5	84.92(6)	C9	C12	N2	123.01(18)
N6	Co2	O6	84.38(6)	C14	C13	N6	123.07(18)
N6	Co2	O8	92.23(6)	C15	C14	C13	119.85(19)
N6	Co2	N2	86.52(6)	C16	C15	C14	116.99(18)
N7	Co2	O5	88.49(6)	C241	C15	C14	119.92(18)
N7	Co2	O6	90.28(6)	C241	C15	C16	123.10(17)
N7	Co2	O8	93.95(6)	C15	C16	C6	119.49(19)
N7	Co2	N2	96.97(6)	C7	C17	C5	124.85(18)
N7	Co2	N6	173.02(6)	C21	C18	N5	123.15(17)
C36	O1	Co1	121.24(14)	C20	C19	N5	123.36(17)
N3	O2	Co1	89.41(10)	C22	C20	C19	119.76(17)
N3	O3	Co1	94.14(11)	C22	C21	C18	119.98(17)
N8	O5	Co2	93.89(11)	C21	C22	C20	116.69(17)
N8	O6	Co2	90.36(10)	C23	C22	C20	120.21(16)
N9	O8	Co2	123.58(13)	C23	C22	C21	123.09(17)
C1	N1	Co1	124.87(12)	C24	C23	C22	124.33(18)
C2	N1	Co1	117.87(12)	C23	C24	C151	125.13(18)
C2	N1	C1	117.10(15)	C28	C25	N4	123.38(18)
C11	N2	Co2	119.57(12)	C27	C26	N4	123.07(18)
C12	N2	Co2	121.93(13)	C29	C27	C26	119.96(17)
C12	N2	C11	117.16(16)	C29	C28	C25	119.69(18)

O3	N3	O2	116.15(15)	C28	C29	C27	116.94(17)
O10	N3	O2	122.64(17)	C30	C29	C27	119.61(17)
O10	N3	O3	121.21(17)	C30	C29	C28	123.45(18)
C25	N4	Co1	126.04(12)	C31	C30	C29	124.74(18)
C26	N4	Co1	116.99(12)	C32	C31	C30	123.50(18)
C26	N4	C25	116.92(16)	C33	C32	C31	121.43(17)
C18	N5	Co1	121.12(12)	C34	C32	C31	121.66(17)
C19	N5	Co1	121.77(12)	C34	C32	C33	116.90(17)
C19	N5	C18	117.04(16)	C502	C33	C32	119.75(18)
C6	N6	Co2	120.50(13)	C462	C34	C32	119.80(18)
C13	N6	Co2	122.55(13)	C342	C46	N7	123.42(18)
C13	N6	C6	116.95(17)	C332	C50	N7	123.34(18)
C46	N7	Co2	120.84(12)	O12	N10	O11	119.06(17)
C50	N7	Co2	122.29(13)	O13	N10	O11	118.96(16)
C50	N7	C46	116.76(16)	O13	N10	O12	121.98(17)

[1]1-X,1-Y,1-Z; [2]2-X,-Y,2-Z

Table S4. Hydrogen bond geometry (Å, º) for **CoBpe**

D	**H**	**A**	**d(D-H)/Å**	**d(H-A)/Å**	**d(D-A)/Å**	**D-H-A/°**
O1	H35	O11	0.85(3)	1.76(3)	2.604(2)	173(3)

Table S5. Bond lengths (Å) observed for **NiBpe**

Atom	**Atom**	**Length/Å**	**Atom**	**Atom**	**Length/Å**
Ni1	O1	2.0262(14)	C2	C4	1.382(2)
Ni1	O2	2.1704(13)	C3	C5	1.393(2)
Ni1	O3	2.1179(14)	C4	C5	1.394(2)
Ni1	N1	2.0668(13)	C5	C7	1.471(2)
Ni1	N2	2.0716(14)	C6	C7	1.331(3)
Ni1	N9[1]	2.0999(14)	C6	C9	1.466(2)
Ni2	O7	2.0789(13)	C8	C9	1.396(2)
Ni2	O8	2.1498(12)	C8	C11	1.379(2)
Ni2	O9	2.0482(12)	C9	C10	1.394(2)
Ni2	N5	2.0639(13)	C10	C12	1.381(2)
Ni2	N7	2.0879(13)	C14	C16	1.375(2)
Ni2	N10[2]	2.0970(14)	C15	C17	1.384(2)
O1	N3	1.278(2)	C16	C18	1.400(2)
O2	N4	1.275(2)	C17	C18	1.396(2)
O3	N4	1.2756(18)	C18	C19	1.463(2)
O4	N3	1.241(2)	C19	C20	1.334(2)
O5	N3	1.228(2)	C20	C21	1.467(2)

O6	N4	1.222(2)	C21	C22	1.389(3)
O7	N6	1.2763(17)	C21	C23	1.397(2)
O8	N6	1.278(2)	C22	C24	1.379(2)
O9	C13	1.428(2)	C23	C25	1.378(2)
O10	N6	1.218(2)	C26	C29	1.377(2)
N1	C1	1.347(2)	C27	C28	1.379(2)
N1	C2	1.342(2)	C28	C30	1.393(2)
N2	C26	1.338(2)	C29	C30	1.389(2)
N2	C27	1.348(2)	C30	C31	1.470(2)
N5	C11	1.346(2)	C31	C32	1.325(2)
N5	C12	1.342(2)	C32	C34	1.469(2)
N7	C14	1.343(2)	C33	C34	1.398(2)
N7	C15	1.3451(19)	C33	C36	1.376(2)
N9	C24	1.344(2)	C34	C35	1.395(2)
N9	C25	1.338(2)	C35	C37	1.382(2)
N10	C36	1.345(2)	O11	N8	1.242(2)
N10	C37	1.347(2)	O12	N8	1.231(2)
C1	C3	1.379(2)	O13	N8	1.2781(18)

[1]1-X,1-Y,1-Z; [2]2-X,-Y,2-Z

Table S6. Bond angles (º) observed for **NiBpe**

Atom	**Atom**	**Atom**	**Angle/°**	**Atom**	**Atom**	**Atom**	**Angle/°**
O1	Ni1	O2	111.39(5)	C24	N9	Ni1[1]	121.94(12)
O1	Ni1	O3	171.93(5)	C25	N9	Ni1[1]	121.39(11)
O1	Ni1	N1	88.27(6)	C25	N9	C24	116.67(15)
O1	Ni1	N2	91.76(6)	C36	N10	Ni2[2]	117.50(11)
O1	Ni1	N9[1]	92.25(6)	C36	N10	C37	116.74(14)
O3	Ni1	O2	60.55(5)	C37	N10	Ni2[2]	125.72(12)
N1	Ni1	O2	159.03(6)	N1	C1	C3	123.22(16)
N1	Ni1	O3	99.68(5)	N1	C2	C4	122.91(17)
N1	Ni1	N2	96.61(5)	C1	C3	C5	119.41(17)
N1	Ni1	N9[1]	87.11(5)	C2	C4	C5	119.67(17)
N2	Ni1	O2	90.21(5)	C3	C5	C4	117.40(15)
N2	Ni1	O3	88.74(6)	C3	C5	C7	121.57(16)
N2	Ni1	N9[1]	174.61(6)	C4	C5	C7	121.03(16)
N9[1]	Ni1	O2	84.97(5)	C7	C6	C9	125.08(17)
N9[1]	Ni1	O3	86.78(6)	C6	C7	C5	123.25(17)
O7	Ni2	O8	61.54(5)	C11	C8	C9	119.92(15)
O7	Ni2	N7	88.08(5)	C8	C9	C6	119.14(15)
O7	Ni2	N10[2]	92.35(5)	C10	C9	C6	123.78(16)
O9	Ni2	O7	159.79(5)	C10	C9	C8	117.06(14)
O9	Ni2	O8	98.33(5)	C12	C10	C9	119.50(16)
O9	Ni2	N5	103.34(5)	N5	C11	C8	122.72(16)

O9	Ni2	N7	88.80(5)	N5	C12	C10	123.22(15)
O9	Ni2	N10[2]	90.13(5)	N7	C14	C16	123.49(14)
N5	Ni2	O7	96.73(5)	N7	C15	C17	122.64(15)
N5	Ni2	O8	158.24(6)	C14	C16	C18	119.70(15)
N5	Ni2	N7	92.35(5)	C15	C17	C18	120.14(14)
N5	Ni2	N10[2]	89.52(5)	C16	C18	C19	123.01(15)
N7	Ni2	O8	86.06(5)	C17	C18	C16	116.68(14)
N7	Ni2	N10[2]	178.02(5)	C17	C18	C19	120.30(14)
N10[2]	Ni2	O8	92.44(5)	C20	C19	C18	124.42(15)
N3	O1	Ni1	124.70(13)	C19	C20	C21	125.14(16)
N4	O2	Ni1	90.45(9)	C22	C21	C20	119.98(15)
N4	O3	Ni1	92.83(11)	C22	C21	C23	117.08(16)
N6	O7	Ni2	92.72(10)	C23	C21	C20	122.94(17)
N6	O8	Ni2	89.46(9)	C24	C22	C21	119.79(17)
C13	O9	Ni2	120.83(11)	C25	C23	C21	119.20(17)
C1	N1	Ni1	119.69(11)	N9	C24	C22	123.33(17)
C2	N1	Ni1	121.69(12)	N9	C25	C23	123.92(16)
C2	N1	C1	117.34(14)	N2	C26	C29	123.61(15)
C26	N2	Ni1	121.35(11)	N2	C27	C28	123.13(16)
C26	N2	C27	116.75(14)	C27	C28	C30	119.82(15)
C27	N2	Ni1	121.73(11)	C26	C29	C30	119.81(15)
O4	N3	O1	117.69(18)	C28	C30	C31	121.34(15)
O5	N3	O1	118.61(19)	C29	C30	C28	116.87(15)
O5	N3	O4	123.70(18)	C29	C30	C31	121.76(15)
O2	N4	O3	115.95(15)	C32	C31	C30	123.71(15)
O6	N4	O2	122.58(16)	C31	C32	C34	124.76(15)
O6	N4	O3	121.46(18)	C36	C33	C34	120.00(16)
C11	N5	Ni2	117.62(11)	C33	C34	C32	119.51(16)
C12	N5	Ni2	124.86(11)	C35	C34	C32	123.83(15)
C12	N5	C11	117.44(13)	C35	C34	C33	116.66(15)
O7	N6	O8	115.84(14)	C37	C35	C34	119.82(16)
O10	N6	O7	121.23(16)	N10	C36	C33	123.40(15)
O10	N6	O8	122.92(15)	N10	C37	C35	123.34(16)
C14	N7	Ni2	121.02(10)	O11	N8	O13	119.07(15)
C14	N7	C15	117.32(13)	O12	N8	O11	121.81(16)
C15	N7	Ni2	121.58(11)	O12	N8	O13	119.11(16)

[1]1-X,1-Y,1-Z; [2]2-X,-Y,2-Z

Table S7. Hydrogen bond geometry (Å, º) for **NiBpe**

D	**H**	**A**	**d(D-H)/Å**	**d(H-A)/Å**	**d(D-A)/Å**	**D-H-A/°**
O9	H9	O13	0.84	1.78	2.6179(17)	171(1)

Table S8. Bond lengths (Å) observed for **CuBpe**

Atom	Atom	Length/Å	Atom	Atom	Length/Å
Cu1	Cu1[1]	2.6182(5)	C9	O2A	1.260(9)
Cu1	O4A[1]	1.982(9)	C7	C8	1.501(3)
Cu1	O2B[1]	1.985(9)	C7	O3B	1.266(10)
Cu1	O3A	1.985(9)	C7	O4B	1.257(9)
Cu1	O1B	1.983(8)	C1B	C2B	1.375(16)
Cu1	N1B	2.16(2)	C5B	C4B	1.384(17)
Cu1	N1A	2.18(3)	C4B	C3B	1.402(8)
Cu1	O1A	1.986(9)	C2B	C3B	1.374(9)
Cu1	O2A[1]	1.981(9)	C3B	C6B	1.465(8)
Cu1	O3B	1.964(10)	C6B	C6B[2]	1.328(9)
Cu1	O4B[1]	1.973(9)	C6A	C6A[2]	1.325(11)
O4A	C7	1.275(10)	C6A	C3A	1.485(9)
O2B	C9	1.261(9)	C1A	N1A	1.339(11)
O3A	C7	1.263(10)	C1A	C2A	1.40(2)
O1B	C9	1.273(9)	N1A	C5A	1.336(12)
N1B	C1B	1.345(10)	C5A	C4A	1.388(18)
N1B	C5B	1.334(10)	C4A	C3A	1.404(9)
C9	C10	1.509(3)	C3A	C2A	1.354(9)
C9	O1A	1.266(9)			

[1]1-X,1-Y,1-Z; [2]2-X,2-Y,-Z

Table S9. Bond angles (º) observed for **CuBpe**

Atom	Atom	Atom	Angle/°	Atom	Atom	Atom	Angle/°
O4A[1]	Cu1	O3A	166.1(5)	O2B	C9	O1B	125.5(7)
O4A[1]	Cu1	N1B	93.2(5)	O2B	C9	C10	116.7(6)
O4A[1]	Cu1	O1A	100.2(4)	O1B	C9	C10	117.8(5)
O2B[1]	Cu1	Cu1[1]	83.9(3)	O1A	C9	C10	117.3(5)
O2B[1]	Cu1	N1A	93.8(7)	O2A	C9	C10	117.5(6)
O3A	Cu1	N1B	97.4(5)	O2A	C9	O1A	125.2(8)
O3A	Cu1	O1A	87.5(5)	O4A	C7	C8	116.1(6)
O1B	Cu1	Cu1[1]	84.7(3)	O3A	C7	O4A	126.3(8)
O1B	Cu1	O2B[1]	164.8(4)	O3A	C7	C8	117.6(6)
O1B	Cu1	N1A	97.9(7)	O3B	C7	C8	117.5(6)
N1A	Cu1	Cu1[1]	176.9(5)	O4B	C7	C8	118.7(6)

O1A	Cu1	N1B	97.1(7)	O4B	C7	O3B	123.8(8)
O2A[1]	Cu1	O3A	80.7(5)	N1B	C1B	C2B	124.2(11)
O2A[1]	Cu1	N1B	95.1(6)	N1B	C5B	C4B	123.2(11)
O2A[1]	Cu1	O1A	164.0(4)	C5B	C4B	C3B	119.8(7)
O3B	Cu1	Cu1[1]	84.8(4)	C3B	C2B	C1B	119.7(7)
O3B	Cu1	O4A[1]	169.1(5)	C4B	C3B	C6B	118.6(7)
O3B	Cu1	O2B[1]	100.1(5)	C2B	C3B	C4B	116.7(6)
O3B	Cu1	O1B	88.8(5)	C2B	C3B	C6B	124.6(7)
O3B	Cu1	N1A	93.5(6)	C6B[2]	C6B	C3B	126.5(7)
O3B	Cu1	O2A[1]	90.1(5)	C6A[2]	C6A	C3A	126.7(7)
O3B	Cu1	O4B[1]	163.7(5)	N1A	C1A	C2A	121.5(13)
O4B[1]	Cu1	Cu1[1]	82.8(3)	C1A	N1A	Cu1	118.3(13)
O4B[1]	Cu1	O4A[1]	10.0(6)	C5A	N1A	Cu1	123.5(13)
O4B[1]	Cu1	O2B[1]	89.2(4)	C5A	N1A	C1A	118.2(18)
O4B[1]	Cu1	O1B	79.5(4)	N1A	C5A	C4A	123.4(14)
O4B[1]	Cu1	N1A	99.3(5)	C5A	C4A	C3A	117.9(9)
O4B[1]	Cu1	O2A[1]	99.1(4)	C4A	C3A	C6A	121.5(8)
C7	O4A	Cu1[1]	121.9(8)	C2A	C3A	C6A	119.9(8)
C9	O2B	Cu1[1]	122.6(8)	C2A	C3A	C4A	118.6(7)
C7	O3A	Cu1	121.0(8)	C3A	C2A	C1A	120.3(8)
C9	O1B	Cu1	121.1(7)	C9	O1A	Cu1	121.3(7)
C1B	N1B	Cu1	124.3(11)	C9	O2A	Cu1[1]	122.9(8)
C5B	N1B	Cu1	119.4(11)	C7	O3B	Cu1	122.3(9)
C5B	N1B	C1B	116.3(14)	C7	O4B	Cu1[1]	123.6(8)

[1]1-X,1-Y,1-Z; [2]2-X,2-Y,-Z

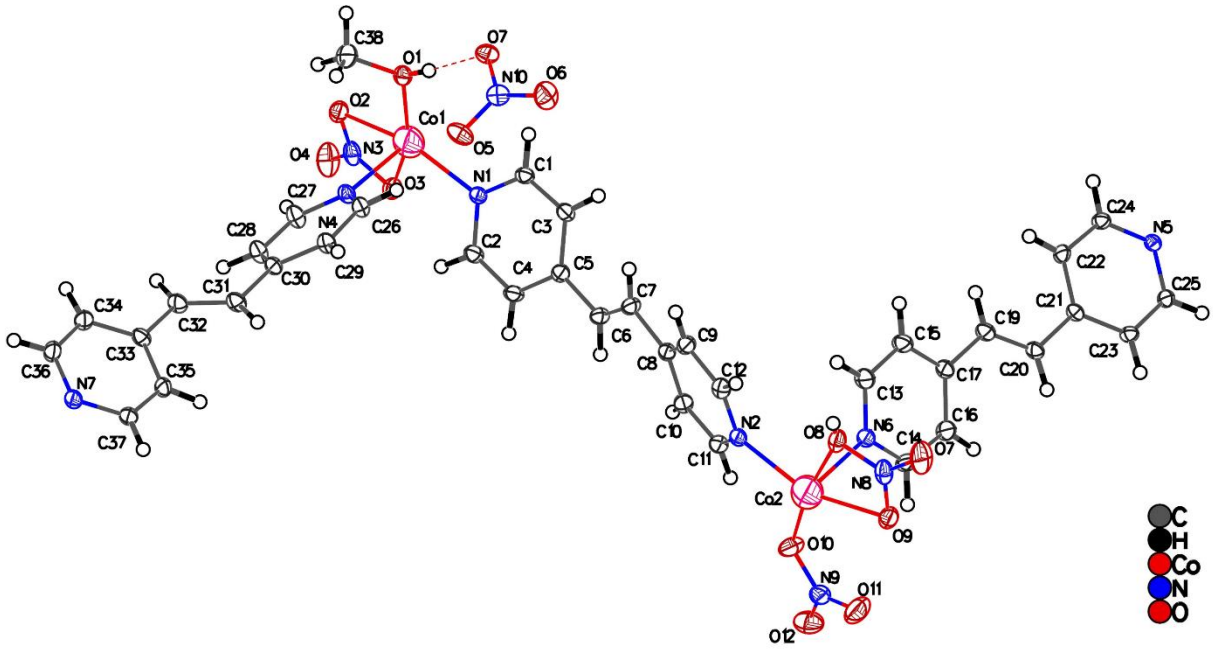

Fig. S1 The solid-state structure of **CoBpe** (ORTEP view, ellipsoid at 50% probability level) with labeled atoms.

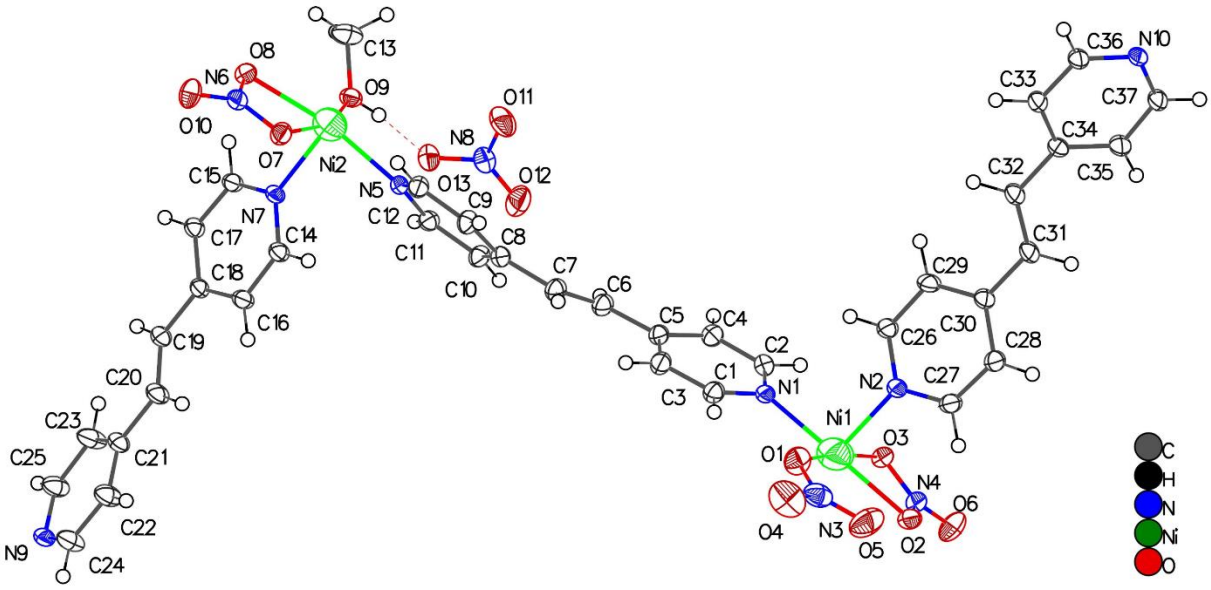

Fig. S2 The solid-state structure of **NiBpe** (ORTEP view, ellipsoid at 50% probability level) with labeled atoms.

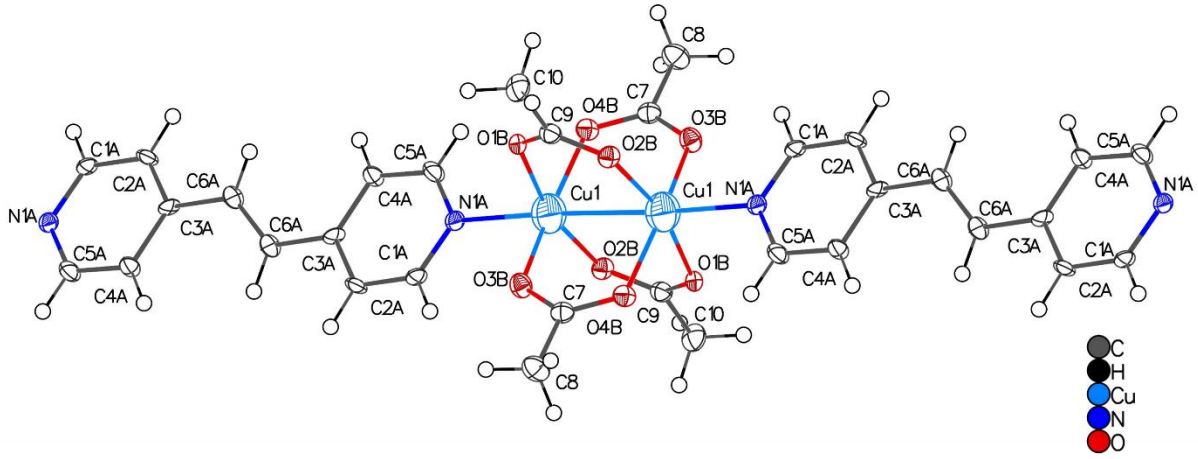

Fig. S3 The solid-state structure of **CuBpe** (ORTEP view, ellipsoid at 50% probability level) with labeled atoms.

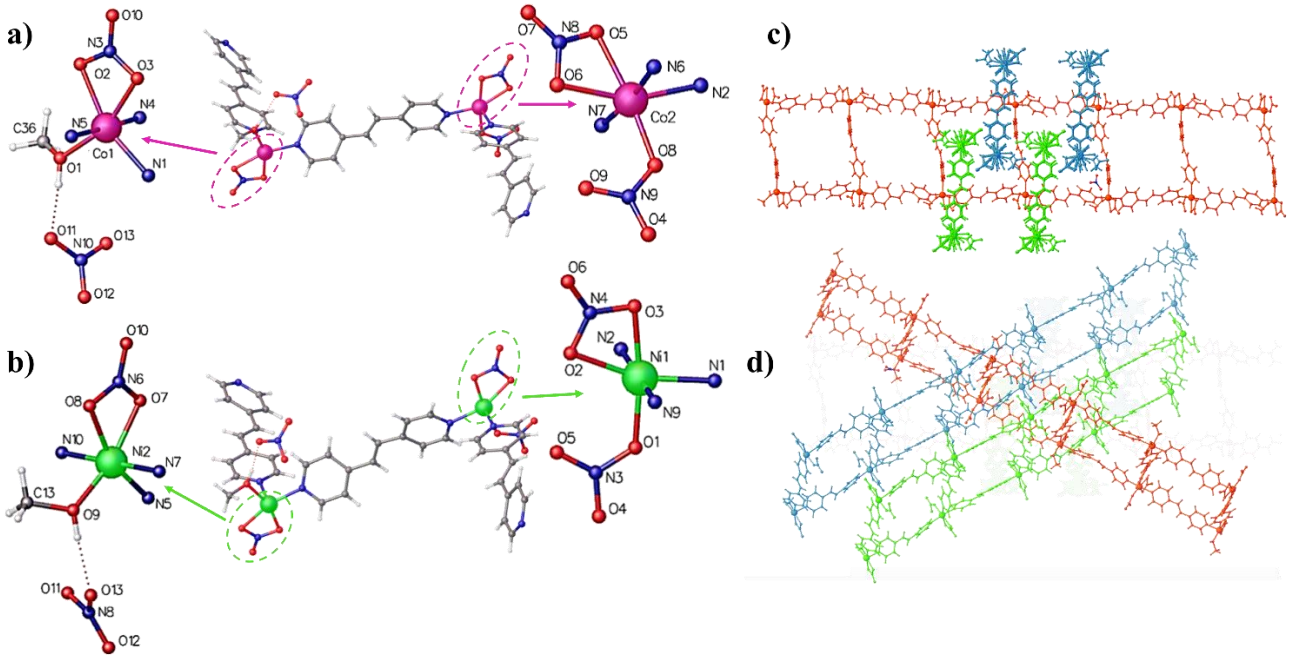

Fig. S4 The solid-state structures of isostructural **CoBpe** and **NiBpe**: a) asymmetric unit (middle), coordination environment of Co(II) cation in **CoBpe** (left & right); b) asymmetric unit (middle), coordination environment of Ni(II) cation in **NiBpe** (left & right); c) view along *a*-axis showing interpenetrated ladders structure : each square grid is interpenetrated with two squares belonging to two other ladders (green & blue) resulting in an overall 3D network d) side view of the 3D ladder structure highlighting the interpenetration of the ladders.

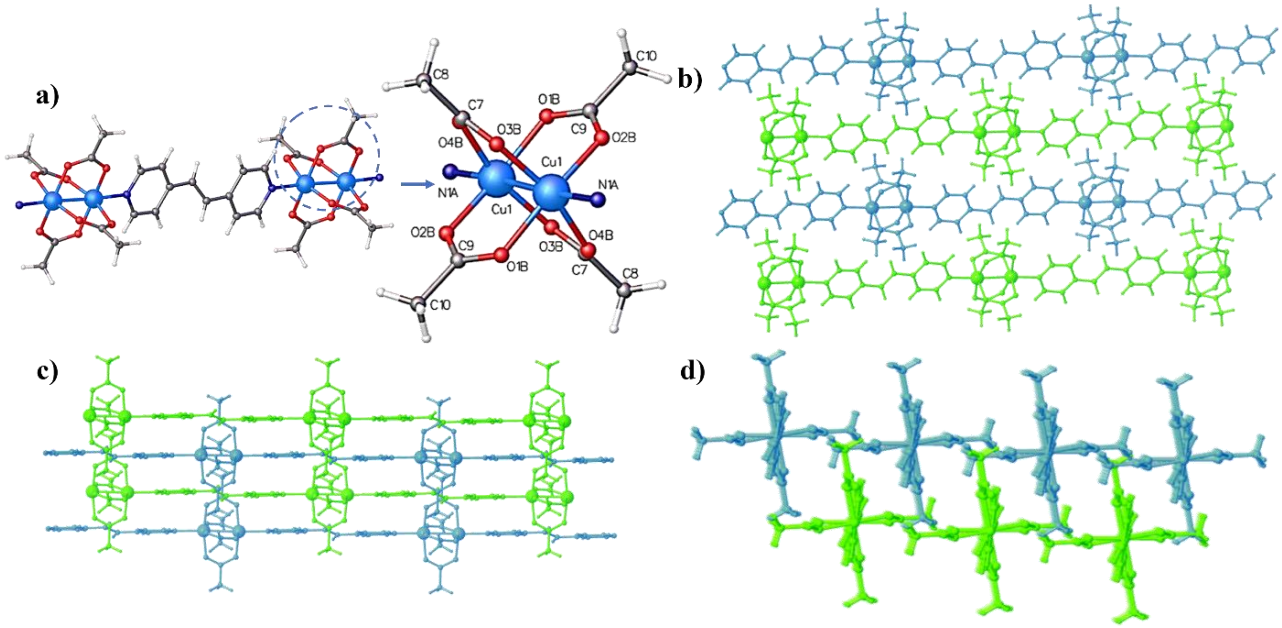

Fig. S5 The solid-state structure of **CuBpe**: a) asymmetric unit (right) and coordination environment of Cu(II) cation (left); b) view along *a*-axis showing periodically alternating 1D channels (green & blue); c) view along *c*-axis showing the arrangement of 1D channels into 2D layers; d) view along *b*-axis showing the alternation of 1D channels.

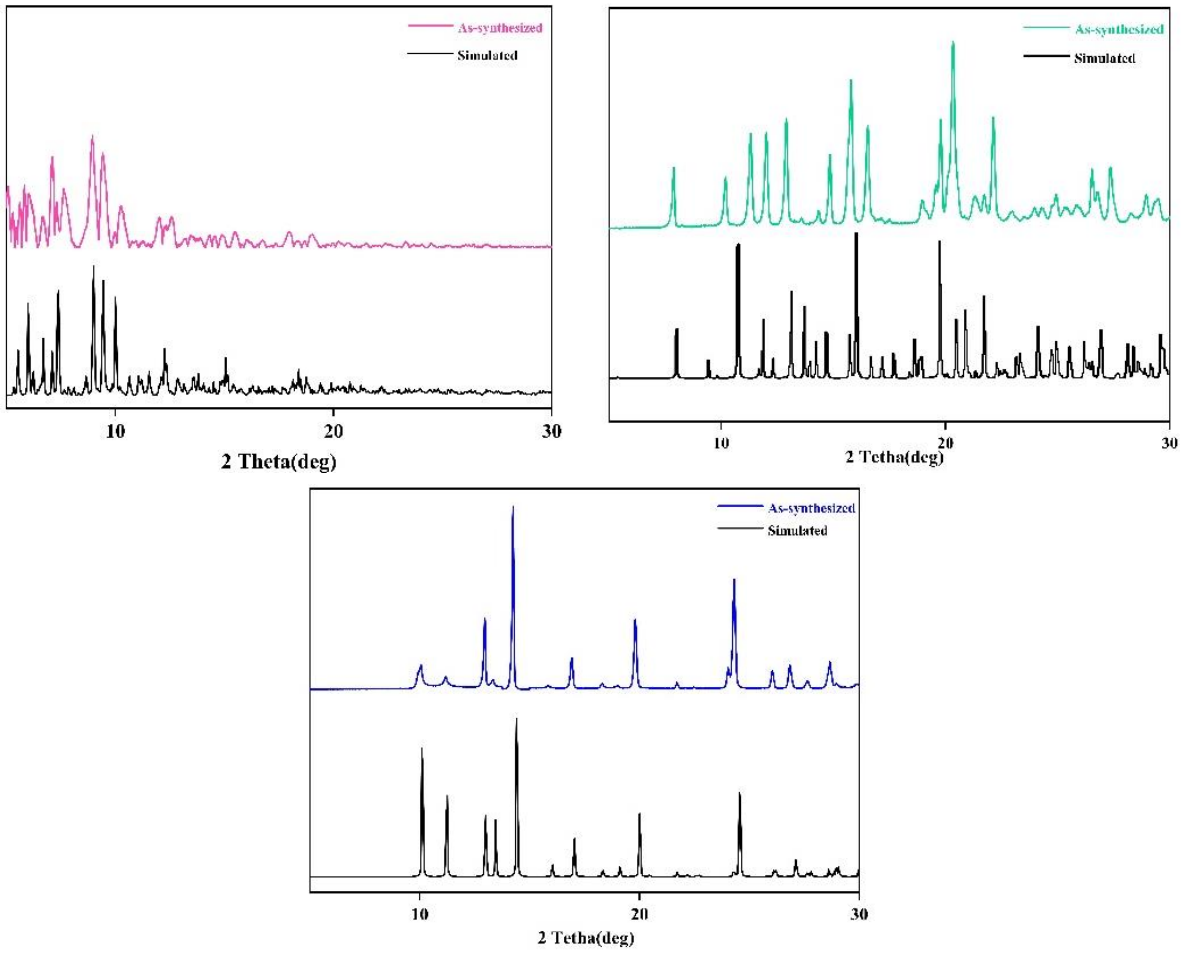

Fig. S6 Experimental powder X-ray diffraction (PXRD) patterns of **CoBpe** (pink), **NiBpe** (green) and **CuBpe** (blue) – comparison with simulated patterns calculated from the corresponding single-crystal structure (in black).

3. Hirshfeld Surface Analysis (HS)

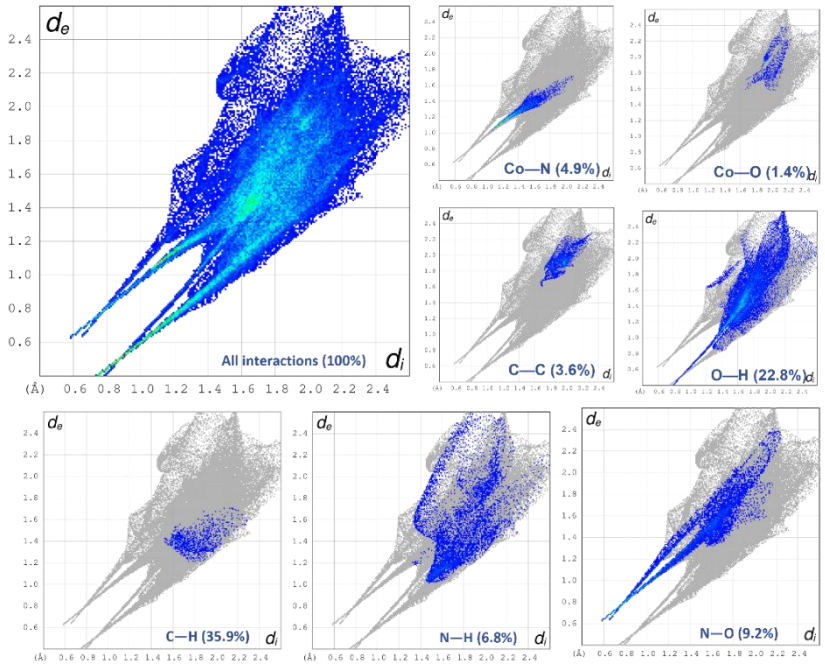

Fig. S7 2D fingerprint plots with relative contributions (in percentage) of various intermolecular contacts to HS area for **CoBpe**.

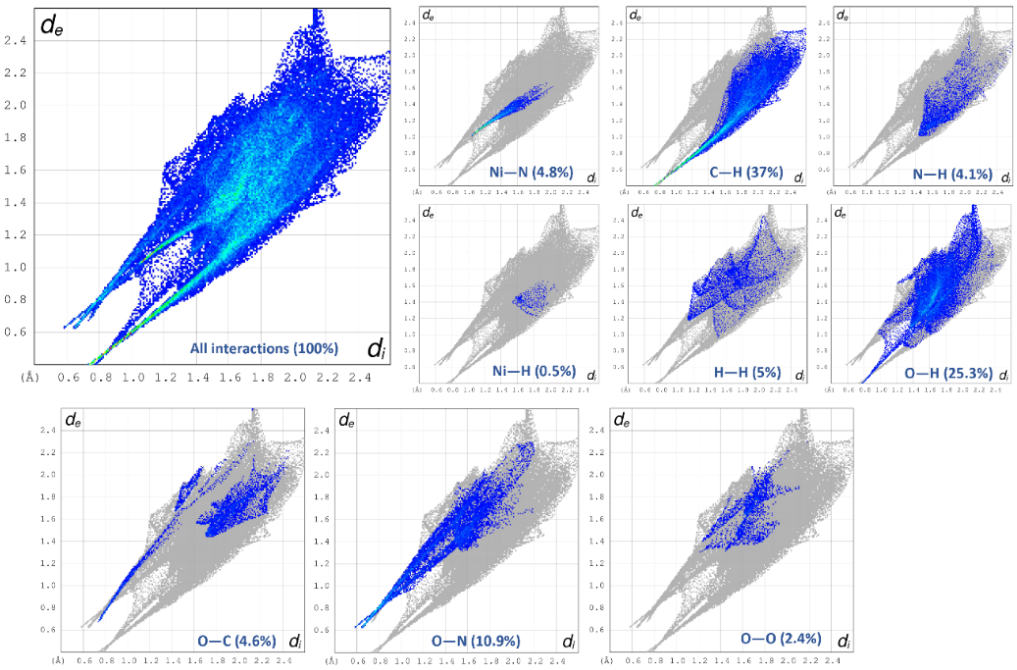

Fig. S8 2D fingerprint plots with relative contributions (in percentage) of various intermolecular contacts to HS area for **NiBpe**.

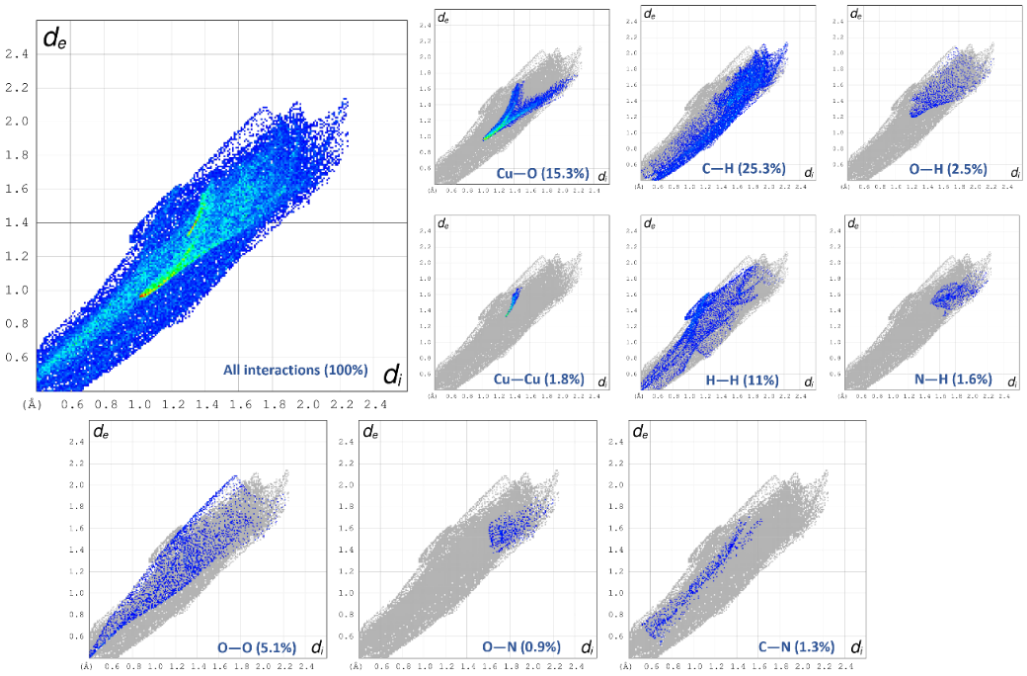

Fig. S9 2D fingerprint plots with relative contributions (in percentage) of various intermolecular contacts to HS area for **CuBpe**.

4. Optical properties

Tauc's plot method. Bandgap energy (Eg) was calculated by **Tauc's plot** method[1] using equation eq.1:

$$\text{Tauc's equation: } (\alpha h\vartheta)^{1/n} = A(h\vartheta - Eg) \qquad \text{eq. (1)}$$

α is the absorption coefficient related to wavelength λ (nm); h is Planck constant; Eg (eV) is the bandgap; ϑ is frequency of light; A is a constant; and **n** is Tauc's coefficient related to the nature of the optical transition type: it can be 1/2 for direct (allowed) transition semiconductor materials or 2 for indirect (non-allowed) transition semiconductor materials; CPs and MOFs are considered as semiconductors with direct band gap 'n=1/2'.[2]Results were obtained by plotting $\mathbf{(\alpha h\vartheta)^{(1/n)}}$ (y-axis) *vs* the photon energy (E = hϑ) (x-axis), **Eg** refers to the intersection point between the tangent line parallel to the linear segment of the curve and x-axis.

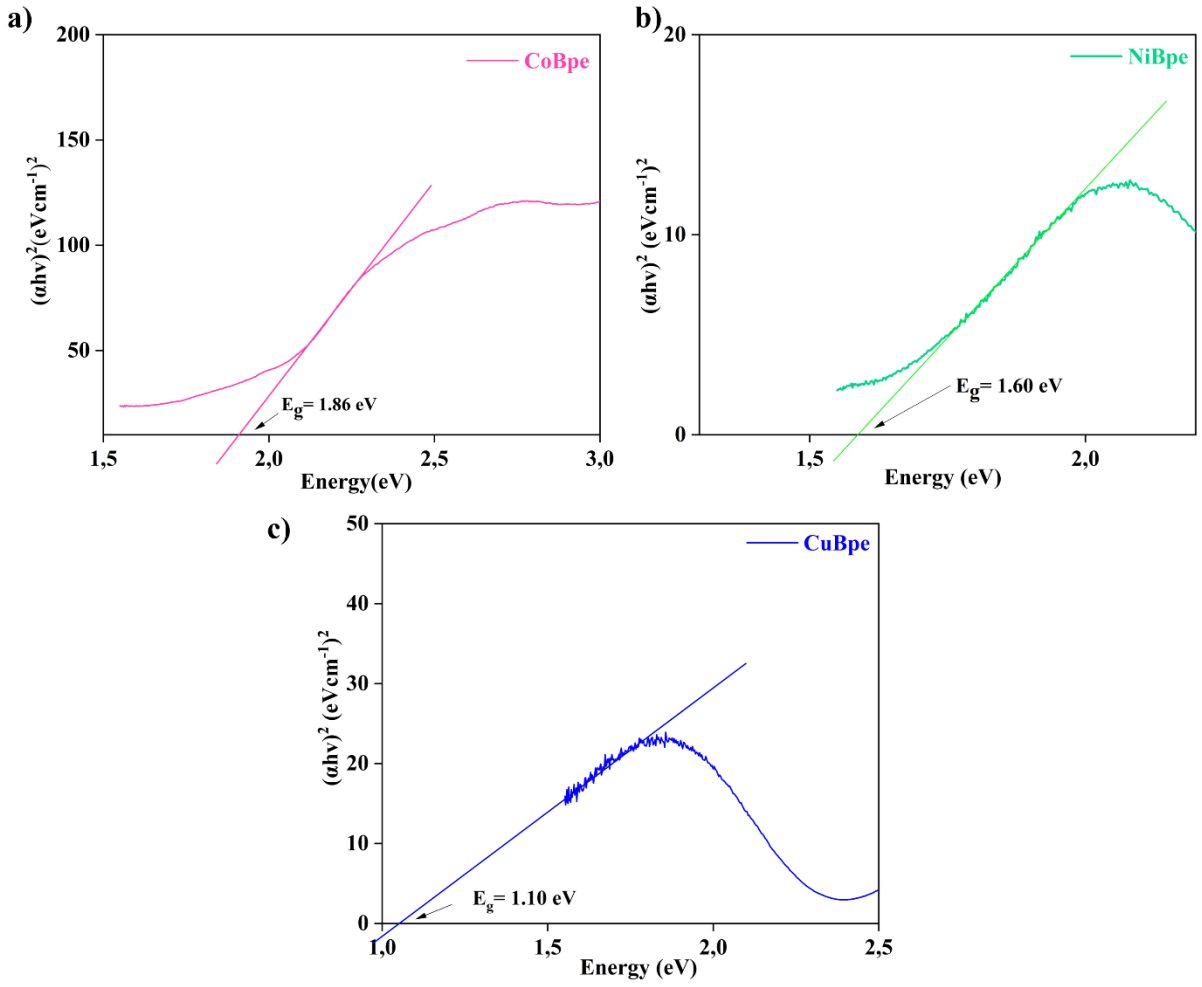

Fig. S10 Tauc's plots for **CoBpe** (pink), **NiBpe** (green) and **CuBpe** (blue).

5. Photoelectrochemical characterization

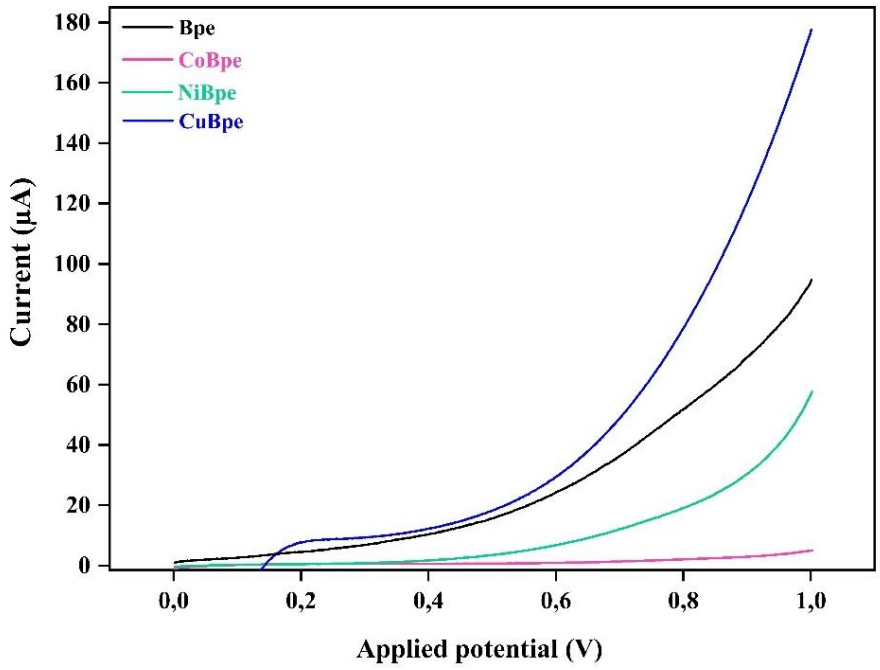

Fig. S11 Linear sweep voltammetry (LSV) curves for **Bpe** (black), **NiBpe** (green), **CoBpe** (pink), **CuBpe** (blue).

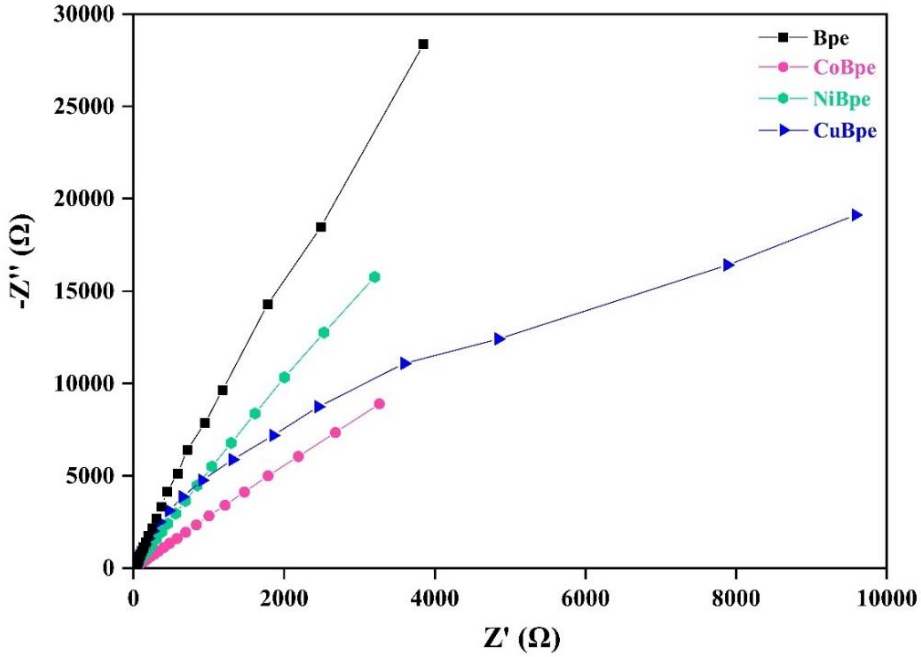

Fig. S12 Nyquist plots for **Bpe** (black), **NiBpe** (green), **CoBpe** (pink), **CuBpe** (blue).

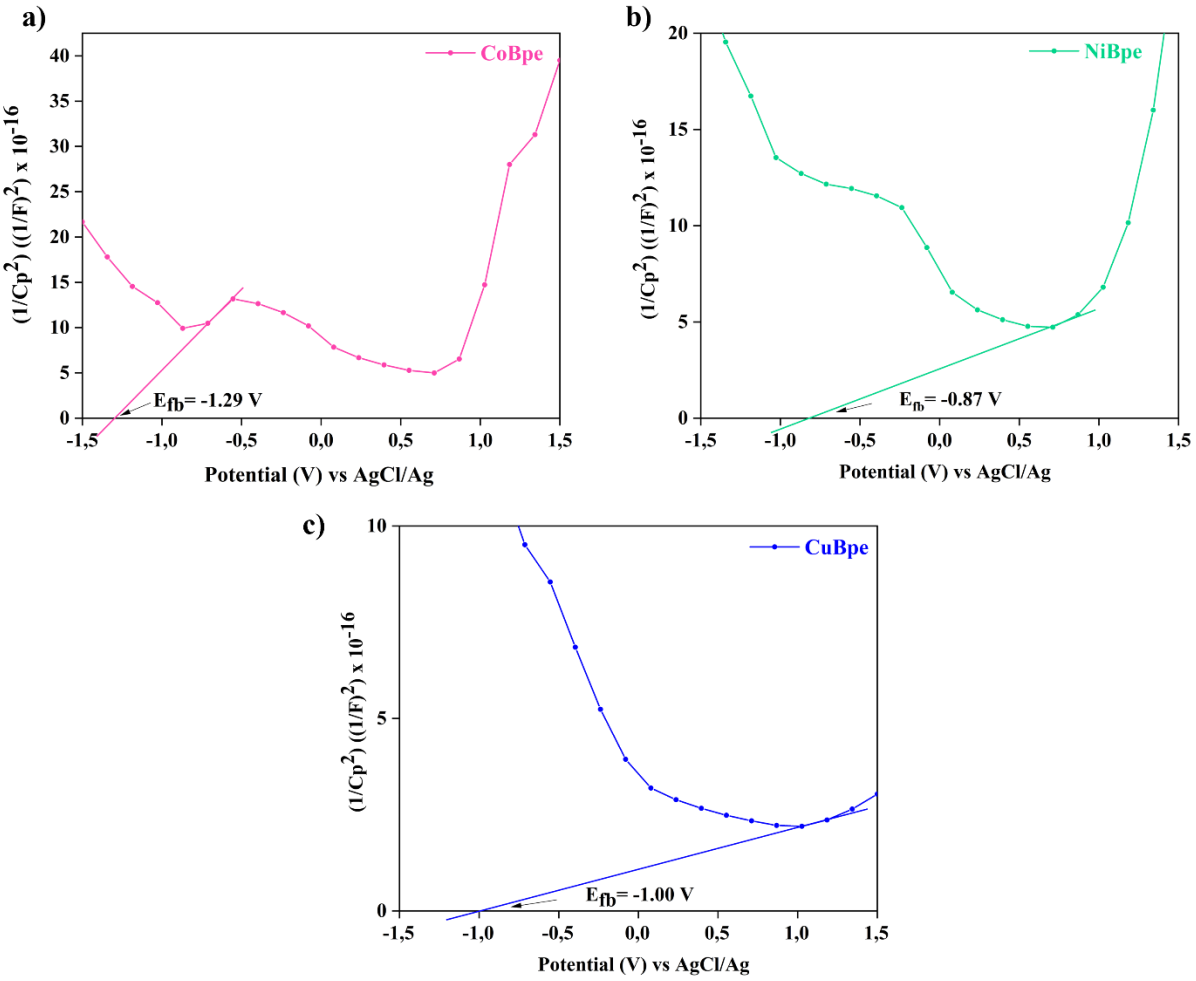

Fig. S13 Mott-Schottky analysis for **CoBpe** (pink), **NiBpe** (green), **CuBpe** (blue).

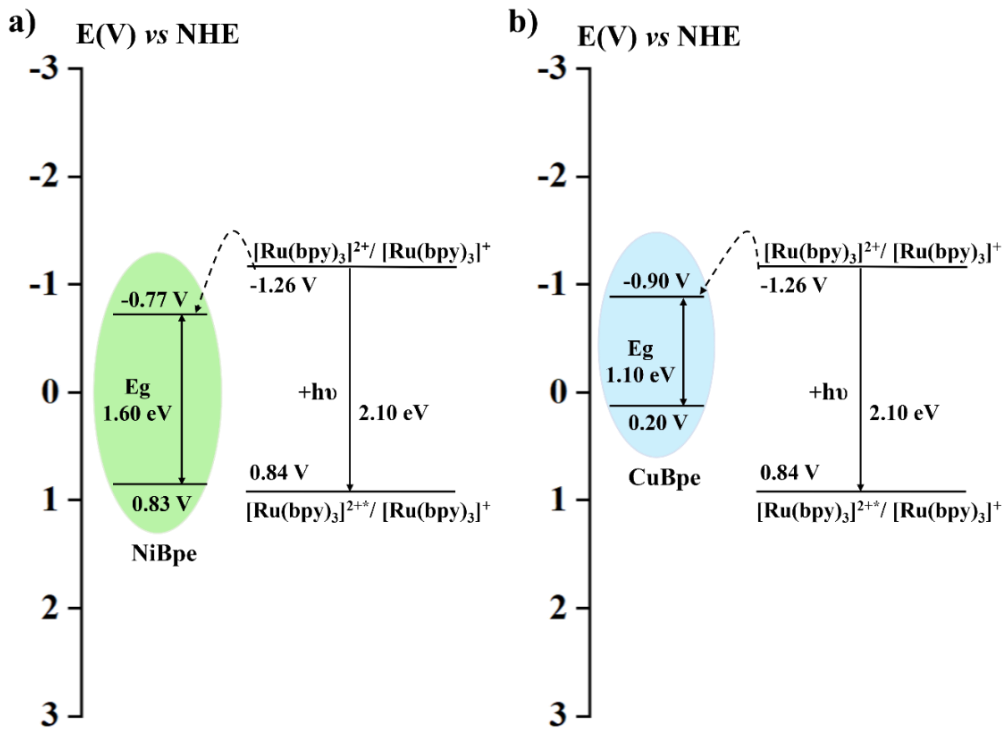

Fig. S14 Electron-transfer diagram for **NiBpe** (a) and **CuBpe** (b), respectively.[3]

6. Photocatalytic CO_2 reduction

Photocatalytic CO_2 reduction reaction

The photocatalytic reduction of CO_2 was carried out in a 40 mL vial, using **CoBpe**, **NiBpe** and **CuBpe** as catalysts, respectively. Example of a typical reaction: catalyst (10 mg) and photosensitizer (7.4 mg) were added to a solution of acetonitrile (6 mL), water (2 mL), TEOA (2 mL). The reaction mixture was sonicated for 1 hour, purged with pure CO_2 (99.99%, Praxair) for 10 minutes, then irradiated (for 4 hours) with artificial sunlight, under continuous stirring. A 0.5 µL sample of gas was extracted from the headspace of the vial and injected into a gas chromatograph (GC) with a thermal conductivity detector (TCD) to detect and quantify the gaseous products (e.g., CO, H_2).

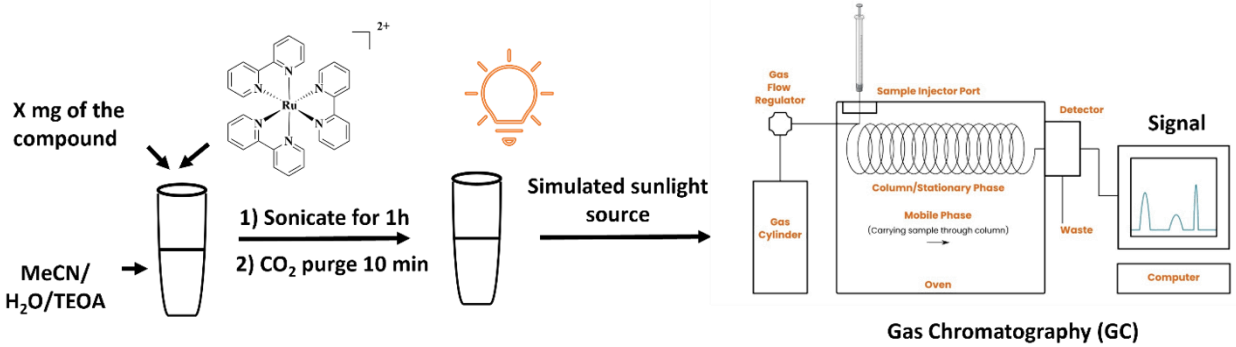

Fig. S15 Photocatalytic experiment: description, conditions, and setup.

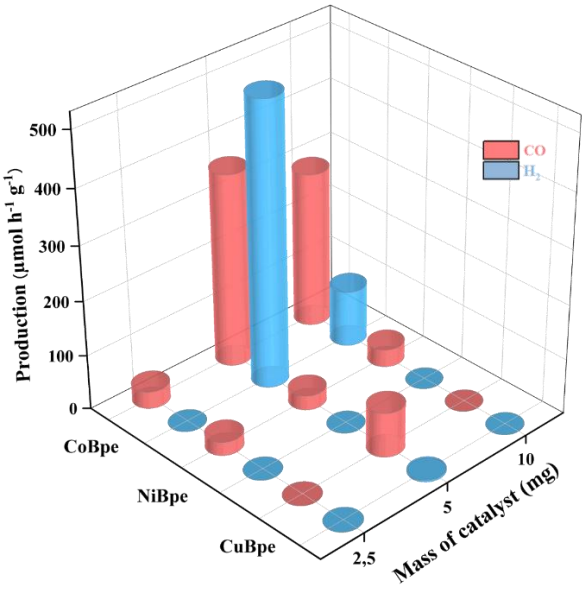

Fig. S16 CO/H_2 production rates for **CoBpe** (top left), **NiBpe** (top right) and **CuBpe** (bottom) as a function of mass of catalyst; 4 hours of simulated sunlight irradiation; $[Ru(bpy)_3]Cl_2 \cdot 6H_2O$ (7.4 mg); $MeCN/H_2O$/TEOA (3/1/1, 10 mL); Experiments were performed at least in duplicate, and the error (1-15%) represents the standard deviation for repeated measurements.

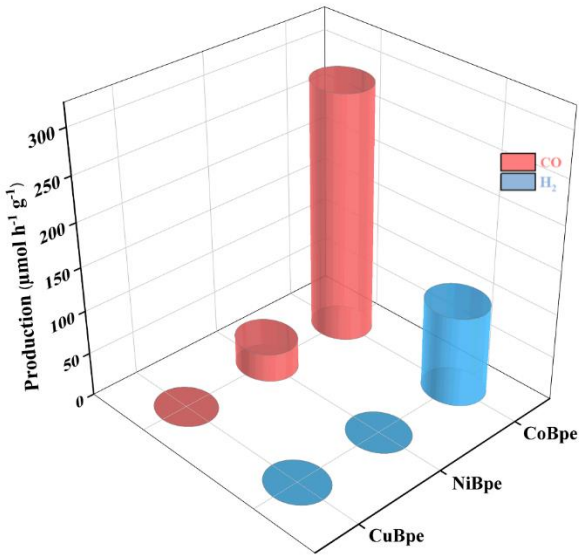

Fig. S17 Photocatalytic CO and H_2 production for **CoBpe**, **NiBpe**, and **CuBpe** (10 mg); 4 hours of simulated sunlight irradiation; $[Ru(bpy)_3]Cl_2 \cdot 6H_2O$ (7.4 mg); $MeCN/H_2O$/TEOA (3/1/1, 10 mL); Experiments were performed at least in duplicate, and the error (1-15%) represents the standard deviation for repeated measurements.

Table S10. Control experiments performed to characterize the activity of **CoBpe** as a catalyst for photocatalytic reduction of CO_2

Catalyst	Reaction conditions	atm	CO ($\mu mol\ g^{-1}\ h^{-1}$)	H_2 ($\mu mol\ g^{-1}\ h^{-1}$)	Sel. CO* (%)
CoBpe	a	CO_2	287	103	74
NiBpe	a	CO_2	33	N/D	100
CuBpe	a	CO_2	N/D**	N/D	N/D
Bpe	a	CO_2	91	33	73
$Co(NO_3)_2 \cdot 6H_2O$	a	CO_2	45	110	29
$Ni(NO_3)_2 \cdot 6H_2O$	a	CO_2	N/D	N/D	N/D
$Cu(ClO_4)_2 \cdot 6H_2O$	a	CO_2	N/D	N/D	N/D
without catalyst	b	CO_2	N/D	N/D	N/D
CoBpe	c	CO_2	N/D	N/D	N/D
CoBpe	d	CO_2	N/D	N/D	N/D
CoBpe	a (3 hours)	Ar	N/D	177	N/D
CoBpe	e	CO_2	31	N/D	100
NiBpe	e	CO_2	25	N/D	100
CuBpe	e	CO_2	N/D	N/D	N/D
CoBpe	f	CO_2	355	520	40
NiBpe	f	CO_2	26	N/D	100
CuBpe	f	CO_2	82	3	95

(a) reaction conditions: catalyst (10 mg), $[Ru(bpy)_3]Cl_2 \cdot 6H_2O$ (7.4 mg), MeCN/H_2O/TEOA (3:1:1, 10 mL); 4 hours of simulated sunlight irradiation.
(b) reaction conditions: same as (a), without catalyst.
(c) reaction conditions: catalyst (10 mg), without photosensitizer $[Ru(bpy)_3]Cl_2 \cdot 6H_2O$, MeCN/$H_2O$/TEOA (3:1:1, 10 mL); 4 hours of simulated sunlight irradiation.
(d) same as (a), in the dark.
*Sel. CO (%) = selectivity of CO (%) = nCO/(nCO + nH_2); nCO = number moles of CO produced; nH_2 = number moles of H_2 produced.
**N/D: not detectable.
(e) reaction conditions: catalyst (2.5 mg), $[Ru(bpy)_3]Cl_2 \cdot 6H_2O$ (7.4 mg), MeCN/H_2O/TEOA (3:1:1, 10 mL); 4 hours of simulated sunlight irradiation.
(f) reaction conditions: catalyst (5 mg), $[Ru(bpy)_3]Cl_2 \cdot 6H_2O$ (7.4 mg), MeCN/H_2O/TEOA (3:1:1, 10 mL); 4 hours of simulated sunlight irradiation.

Table S11. CO production rates for selected relevant reported material-based photocatalytic systems

System	CO ($\mu mol\ g^{-1}\ h^{-1}$)	H_2 ($\mu mol\ g^{-1}\ h^{-1}$)	Sel. CO** (%)	Solvent/SED medium	Ref.
$\{Ni_3(TCA)_2(dpe)_3(H_2O)_6\}_n$*	372	8	98	MeCN/TIPA/ H_2O (3/1/1)	[4]
$\{Co_3(TCA)_2(dpe)_3(H_2O)_6\}_n$*	1140	1265	47		
$\{Cu_3(TCA)_2(dpe)_3(H_2O)_{3n}$*	68	232	23		
CdS@UiO-66-NH_2-3	192	N/D	N/D	H_2O	[5]
COF-366-Co/UiO-66-NH_2*	4092	N/D	73	MeCN/TEOA/ H_2O (3/1/1)	[6]
CoBpe* 4 h/ 8 h	287/ 410	103/ 353	74/ 61	MeCN/TEOA/ H_2O (3/1/1)	this work

TIPA: triisopropanolamine; TEOA: triethanolamine; MeCN: acetonitrile

*$[Ru(bpy)_3]Cl_2 \cdot 6H_2O$ added as photosensitizer

**Sel. CO (%) = selectivity of CO (%) = nCO/(nCO + nH_2); nCO = number moles of CO produced; nH_2 = number moles of H_2 produced.

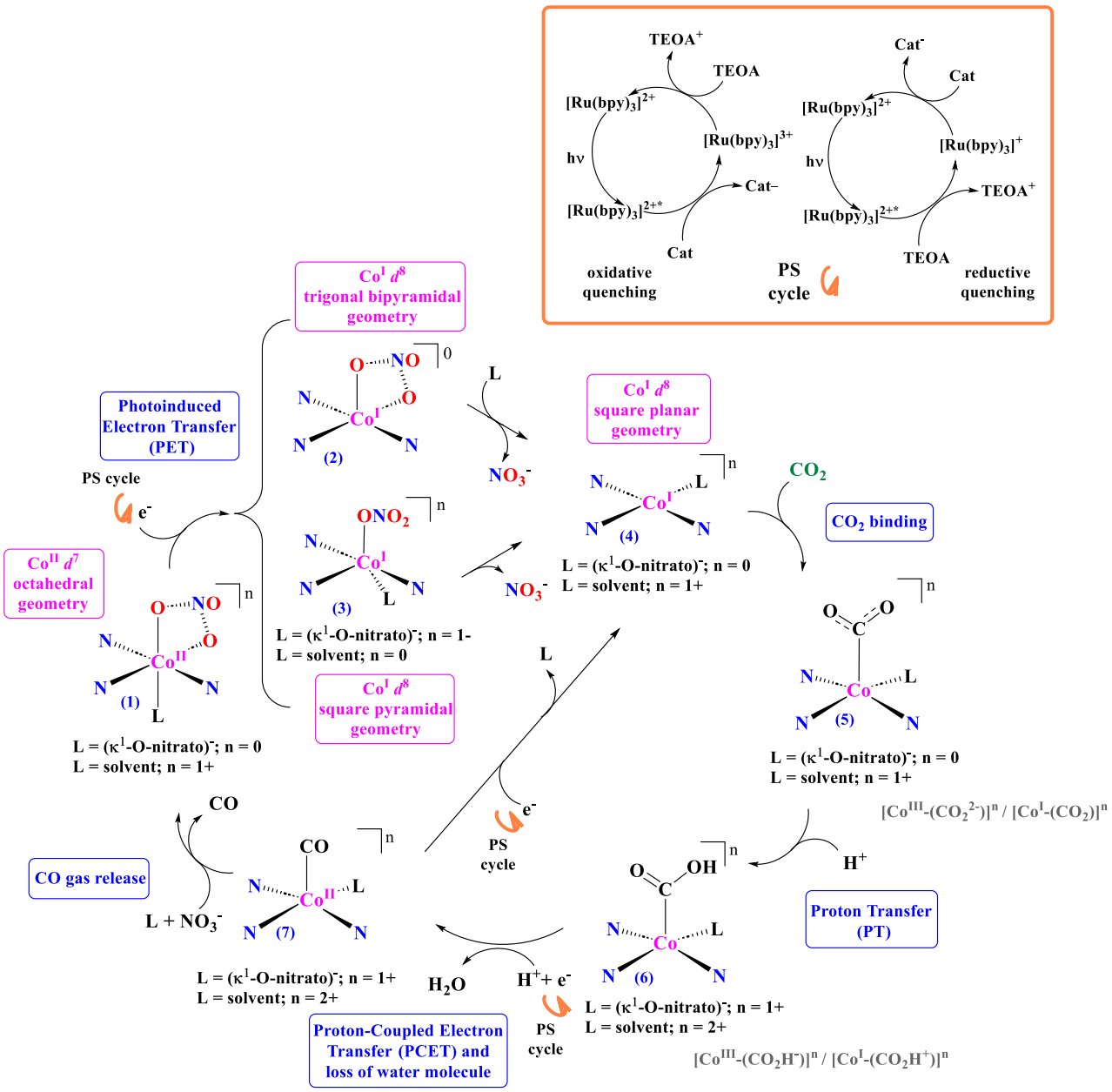

Fig. S18 Proposed photocatalytic mechanism for CO_2 to CO conversion – exemplified for **CoBpe**.

Note to Fig. S18. The cobalt-catalyzed CO_2 reduction mechanism often proceeds *via* the formation of a low-valent Co(I) (d^8) intermediate.[4, 7-11] In the system studied herein, as found in the solid-state structure of CoBpe, there are two distinct cobalt centers, each adopting a distorted octahedral geometry with an MN_3O_3 coordination sphere. In both cases, the three nitrogen atoms from three Bpe ligands (two axial, one equatorial) and the cobalt(II) ion are coplanar, forming a T-shape geometry. In addition, each of the cobalt(II) ions is also coordinated to a nitrate anion in a bidentate fashion (κ^2-O). In the sixth coordination position around the cobalt centers, in one case, a solvent molecule (methanol) is found, while in the second case, a nitrate ion is present, coordinated in a monodentate fashion (κ-O).

Upon light irradiation, an electron is injected from the photosensitizer (PS) cycle to the conduction band (CB) of the CoBpe coordination polymer. Thus, the Co(II) center (d^7, octahedral; structure (1)) is reduced to a low-valent Co(I) species (d^8). For such species, a tetra-coordinated square planar geometry is favored on electronic grounds (structure (4)). Penta-coordinated square pyramidal (structure (2)) or trigonal bipyramidal (structure (3)) geometries are also possible. To achieve these geometries, the labile ligands coordinated to the metal center, such as solvent molecules and coordinated nitrate ions dissociate.

The square planar geometry of Co(I) is well-documented as favorable for d^8 metal centers and plays a crucial role in enabling CO_2 activation.[4, 7-11] In the mechanism proposed herein, Co(I) serves as the active catalytic site for CO_2 binding, allowing the formation of Co-CO_2 adduct (structure (5)). The subsequent proposed steps for CO_2 reduction are in line with mechanistic pathways previously reported:[4, 8-11] a proton transfer (structure (6)); a second one-electron injection (from the PS cycle) coupled (or not) with a second proton transfer and the leaving of a water molecule; and the formation of the Co(II)-CO adduct (structure (7)), followed by the CO decoordination as CO gas. In some reports involving molecular catalysts,[9, 12] the second one-electron reduction is proposed to be concerted with the CO_2 binding, followed by a first proton transfer, and a second proton transfer concerted with the leaving of the water molecule to form the Co-CO adduct. While all these proposals are plausible, we chose to base ours on the reports describing coordination-polymer-based heterogeneous systems,[4, 8, 10, 11] as they are the closest to the ones studied herein.

For the description of structures (5) and (6), two cases can be accepted in absence of information on electron density distribution, as presented in the Fig. S18 (in gray)).

With respect to the photosensitizer (PS) cycle, based on the redox potentials of the species involved in this study (especially when using the CoBpe as catalyst), the role of TEOA as a reductive quencher is more plausible. Thus, in a reductive quenching for the photosensitizer (PS) cycle, the TEOA transfers an electron to the $[Ru(bpy)_3]^{2+*}$ (photoexcited PS (PS^*)), forming $[Ru(bpy)_3]^{+}$ (reduced PS (PS^-)), which further transfers the electron to the catalyst and returns to the ground state $[Ru(bpy)_3]^{2+}$. Literature reports on similar heterogeneous system for CO_2-to-CO photoeduction,[4, 10, 11] put forward the proposal of an oxidative quenching for the PS cycle, where the PS^*, $[Ru(bpy)_3]^{2+*}$ transfers an electron to the coordination polymer catalyst and becomes $[Ru(bpy)_3]^{3+}$ (oxidized PS (PS^+)). The TEOA serves in this case to reduce the $[Ru(bpy)_3]^{3+}$ species to the initial $[Ru(bpy)_3]^{2+}$. Both pathways are presented in Fig. S18 (orange inset).

7. References

1. P. Makuła, M. Pacia and W. Macyk, *Journal*, 2018, **9**, 6814-6817.
2. K. Fabrizio, K. N. Le, A. B. Andreeva, C. H. Hendon and C. K. Brozek, *ACS Materials Letters*, 2022, **4**, 457-463.
3. C. Bock, J. Connor, A. Gutierrez, T. J. Meyer, D. Whitten, B. Sullivan and J. Nagle, *Journal of the American Chemical Society*, 1979, **101**, 4815-4824.
4. X.-K. Wang, J. Liu, L. Zhang, L.-Z. Dong, S.-L. Li, Y.-H. Kan, D.-S. Li and Y.-Q. Lan, *ACS Catalysis*, 2019, **9**, 1726-1732.
5. H.-N. Wang, Y.-H. Zou, Y.-M. Fu, X. Meng, L. Xue, H.-X. Sun and Z.-M. Su, *Nanoscale*, 2021, **13**, 16977-16985.

6. T.-A. Quach, V. N. Gopalakrishnan, J. Becerra, D.-T. Nguyen, J. M. Ahad, S. Mohan and T.-O. Do, *Catalysis Today*, 2023, **421**, 114218.
7. C. E. Housecroft, Sharpe, A. G. , *Inorganic Chemistry, 4th Edition, Pearson, Harlow, p. 639-777* 2012.
8. J. E. Pander III, A. Fogg and A. B. Bocarsly, *ChemCatChem*, 2016, **8**, 3536-3545.
9. A. Call, M. Cibian, K. Yamamoto, T. Nakazono, K. Yamauchi and K. Sakai, *Acs Catalysis*, 2019, **9**, 4867-4874.
10. S.-L. Xie, J. Liu, L.-Z. Dong, S.-L. Li, Y.-Q. Lan and Z.-M. Su, *Chemical science*, 2019, **10**, 185-190.
11. J. He, J. Wang, Y. Chen, J. Zhang, D. Duan, Y. Wang and Z. Yan, *Chemical communications*, 2014, **50**, 7063-7066.
12. A. Call, M. Cibian, K. Yamauchi and K. Sakai, *Sustainable Energy & Fuels*, 2022, **6**, 2160-2164.